Observation and Identification of W^{19+}-W^{23+} Spectra in the EUV Wavelength Region in the Vicinity of 200 Å

Ryota NISHIMURA, Tetsutarou OISHI, Izumi MURAKAMI[1,2)], Daiji KATO[1,3)], Hiroyuki A SAKAUE[1)], Shivam GUPTA[1)], Hayato OHASHI[4)], Motoshi GOTO[1,2)], Yasuko KAWAMOTO[1,2)], Tomoko KAWATE[1,2)], Hiroyuki TAKAHASHI and Kenji TOBITA

Department of Quantum Science and Energy Engineering, Tohoku University, Sendai 980-8579, Japan
[1)]*National Institute for Fusion Science, National Institutes of Natural Sciences, Toki 509-5292, Japan*
[2)]*The Graduate University for Advanced Studies, SOKENDAI, Toki 509-5292, Japan*
[3)]*Interdisciplinary Graduate School of Engineering Sciences, Kyusyu University, Kasuga 816-8580, Japan*
[4)]*Institute of Liberal Arts and Sciences, University of Toyama, Toyama 930-8555, Japan*

(Received 25 April 2024 / Accepted 29 May 2024)

Tungsten (W) is one of the major impurities in ITER and future DEMO reactors. However, diagnosing ion density, temperature, and spatial distribution for tungsten ions in low charge states such as W^{17+}-W^{27+} is difficult due to a lack of spectral line data. In this study, we observed tungsten Unresolved Transition Array (UTA) spectra around W^{20+} in Large Helical Device. Furthermore, the emission spectra of tungsten ions ranging from W^{19+}-W^{23+} were also measured using Compact electron Beam Ion Trap (CoBIT). Two spectral peaks were detected in the CoBIT experimental setup. Subsequently, these peaks were theoretically identified as 5s-5p and $5p_{3/2}$-5d transitions using Flexible Atomic Code (FAC). The identified peaks are useful for impurity diagnostics of ITER edge plasma.

Keywords: tungsten spectra, impurity diagnostics, flexible atomic code, LHD, atomic process

DOI: 10.1585/pfr.19.1402022

1. Introduction

Tungsten (W) will be used as the plasma-facing components in the divertor and first wall region in magnetically confined fusion devices such as ITER and future DEMO reactors [1, 2]. It is considered that tungsten is one of the major impurities present in high-temperature plasmas. Due to its large atomic number of 74, tungsten ions are not completely ionized even under high-temperature plasmas with a central electron temperature $T_{e0} \sim$ 20 - 30 keV of ITER [3]. The presence of tungsten ions in the plasma leads to a large amount of energy losses through excitation, ionization, and radiation, thus contaminated plasma environment hinders long-pulse operation. Therefore, it is necessary to prevent the accumulation of tungsten ions in core-plasma.

On the other hand, in high-temperature plasmas, tungsten impurity has a wide distribution, with highly charged ions distributed in the core-plasma and charged states with lower ionization distributed in the edge plasma region. Due to its high radiation power, tungsten ions in the edge plasma play an important role. In this way, it is important to measure tungsten ions that cover a wide range of charge states. Spectroscopic measurements have been performed over a wide wavelength range, from Soft X-Ray (SXR) region to visible region for monitoring the different charge states of tungsten impurity. So far, spectroscopic studies of tungsten ions have been conducted using high-temperature fusion plasma devices, such as ASDEX Upgrade [4–6], JT-60U [7–9], JET [10], EAST [11], and Large Helical Device (LHD) [12–14]. In LHD, tungsten ions with a maximum charge state of W^{46+} have been observed in tungsten pellet injection experiments [15]. In addition, spectroscopic studies of tungsten ions have also been conducted using the different Electron Beam Ion Trap (EBIT) devices such as Compact EBIT (CoBIT) [16, 17], SW-EBIT [18], SH-HtscEBIT [19].

Generally, W^{17+}-W^{27+} ions have outermost shell electrons occupying the 4f orbit, resulting in highly complex excited structures and a large number of fine structure energy levels. As a result, a pseudo-continuum spectrum called unresolved transition array (UTA) may be observed [20]. For this reason, there is a lack of spectral line data for W^{17+}-W^{27+} ions on major database, Atomic Spectra Database on National Institute of Standards and Technology (NIST-ASD) [21, 22]. On the other hand, a tungsten UTA spectrum was observed near 200 Å with LHD. It was suggested that W^{6+}-W^{27+} ions are included in the UTA spectrum observed near 200 Å [23]. In this study, we attempted to separate the charge states included in the UTA spectrum near 200 Å to expand the tungsten spectral database and provide spectral data for ITER and future

author's e-mail: nishimura.ryota.s5@dc.tohoku.ac.jp

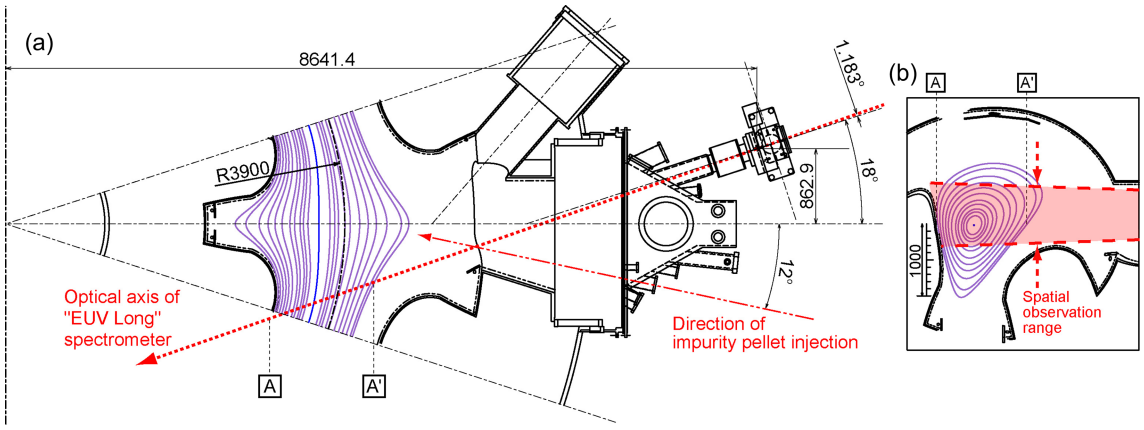

Fig. 1 (a) Top view of LHD with EUV spectrometer and pellet injection system and (b) vertical observation range of EUV spectrometer.

DEMO reactors.

2. Tungsten Pellet Injection Experiment in Large Helical Device

Figure 1 (a) shows the top view of LHD with a Extreme Ultraviolet (EUV) spectrometer and pellet injection system.

In LHD, a tungsten pellet is injected into a high-temperature plasma with a T_{e0} of several keV through the pellet injection port, as shown in Fig. 1 (a). There are some spectrometers that cover a wide wavelength range, but we used a EUV spectrometer named "EUV Long" that covers 50 - 500 Å [24]. The EUV Long spectrometer has 1024 channels in the wavelength direction, and wavelength range of 90 - 290 Å was measured in this study. The wavelength width per channel depends on the wavelength, but it is approximately 0.2 Å at $\lambda \sim 200$ Å. In addition, the wavelength broadening of known line spectra gives the instrumental function, which corresponds to the wavelength resolution. Gaussian fitting of line spectra emitting at around 200 Å, such as Fe XXIV (192.03 Å), gives a wavelength resolution of 0.25 Å of half width at half maximum. The exposure time of the EUV Long spectrometer is 5 ms. The spatial observation range is shown in Fig. 1 (b).

Figure 2 shows the discharge waveforms of (a) plasma heating power, (b) central electron temperature, T_{e0}, (c) central electron density, n_{e0}, (d) plasma stored energy, W_p and (e) radiation power, P_{rad} of tungsten pellet injection experiment in LHD.

In the tungsten pellet experiment, the Electron Cyclotron Heating (ECH) and negative ion source Neutral Beam Injection (n-NBI) heating systems were employed to initiate and maintain the LHD plasma. A tungsten pellet was injected into the plasma with T_{e0} of approximately 3 keV at t ~ 4.1 s. Immediately after the tungsten pellet injection, P_{rad} increased stepwise and then stabilized at a high level, whereas W_p gradually decreased. Due to the ionization of tungsten ions, n_{e0} increased from 2×10^{19} to

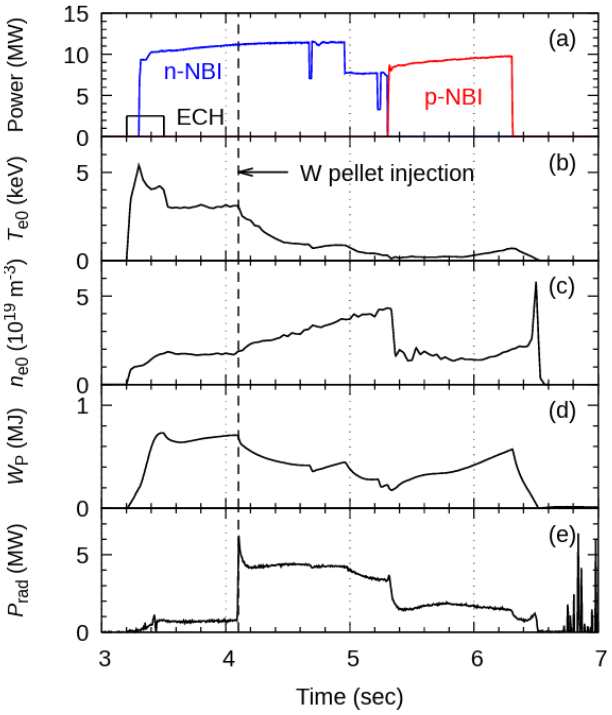

Fig. 2 Discharge waveforms of (a) plasma heating power, (b) central electron temperature, (c) central electron density, (d) plasma stored energy, and (e) radiation power in a tungsten pellet injection experiment in LHD (#170347).

5×10^{19} m^{-3}, whereas T_{e0} decreased from 3 keV to a few hundred eV. Major radial profiles of (a) electron temperature and (b) electron density at 4.9 - 5.3 s are shown in Figs. 3 (a) and (b).

Electron temperature profile in major radial direction, $T_e(R)$, decreased in $R \sim 2.8$ - 4.5 m, while electron density profile, $n_e(R)$, slightly increased. Therefore, tungsten ions are estimated to be mainly located in $R \sim 2.8$ - 4.5 m at t ~ 4.9 - 5.3 s.

EUV spectra near 200 Å observed at t ~ 4.95 - 5.30 s are shown in Fig. 4. Here, the spectra were the summation

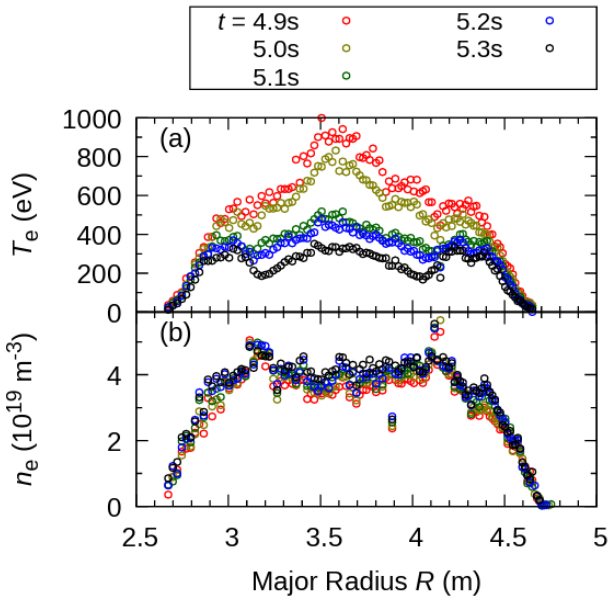

Fig. 3 Radial profiles of (a) electron temperature and (b) electron density at 4.9 - 5.3 s.

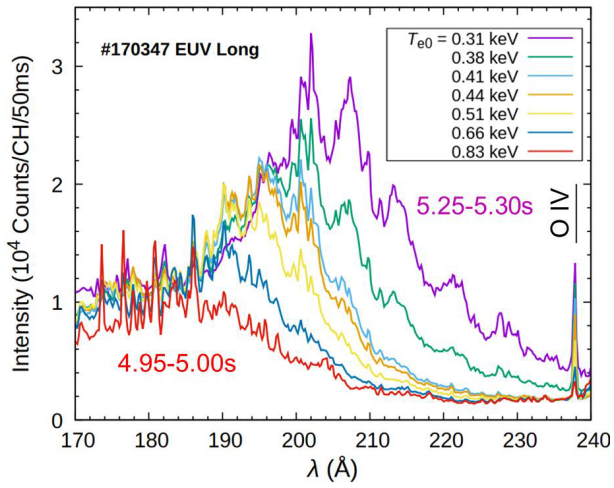

Fig. 4 Measured EUV spectra observed at 4.95 - 5.30 s.

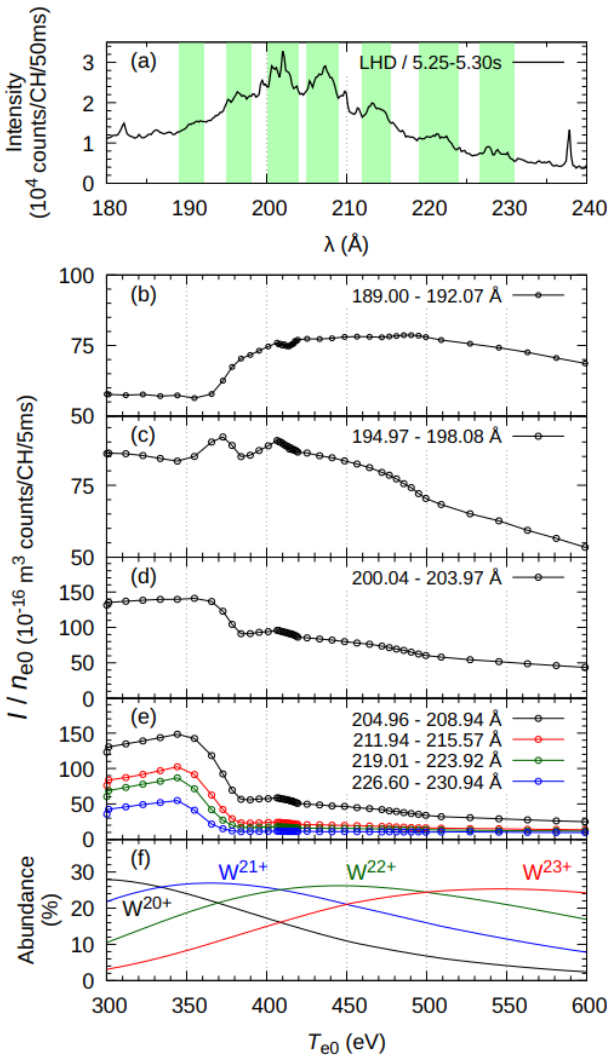

Fig. 5 (a) EUV spectrum at 5.25 - 5.30 s, central electron temperature dependence on integrated line intensity in the wavelength range of (b) 226.60 - 230.94 Å, (c) 219.91 - 223.92 Å, (d) 211.94 - 215.57 Å, (e) 204.96 - 208.94, 200.04 - 203.97, 194.97 - 198.08, 189.00 - 192.07 Å and (f) ion fractional abundance.

on 10 frames (50 ms).

A UTA spectrum was observed within the wavelength range of 170 - 240 Å at t ~ 4.95 - 5.30 s. The spectrum exhibits several pseudo-continuum peaks, including those observed at 192, 196, 202, 208, 214, 220, 228 Å. The UTA spectrum in Fig. 4 was shifted toward longer wavelength region with time. It is considered that the charge state distribution was shifted toward lower charge state with decreasing electron temperature. Notably, a tungsten UTA spectrum measured near 30 Å [16] displays a similar pattern, wherein each peak corresponds to a different charge state. If the UTA spectrum near 200 Å has the similar pattern as the spectrum near 30 Å, it will be useful for monitoring the different charged states of tungsten impurity ions within fusion reactors.

In order to identify the charge state corresponding to each peak, we focused on the dependence of integrated intensity of each peak on T_{e0}. Figures 5 (a), (b)-(e), and (f) show the integrated area of the EUV spectrum observed at t ~ 5.25 - 5.30 s, dependence of integrated intensity of each peak on central electron temperature, T_{e0}, and fractional abundance as a function of electron temperature, respectively.

The region of T_{e0} < 300 eV is not shown in Figs. 5 (b)-(e) because the spectral intensity decreases significantly after switching NBIs from n-NBI to p-NBI (t > 5.3 s). The peaks observed on the short wavelength side, as shown in Figs. 5 (b) and (c), have a high integrated intensity in relatively high electron temperature region of T_{e0} ~ 400 - 450 eV. On the other hand, the peaks observed on the long wavelength side, as shown in Figs. 5 (d) and (e), have

a high integrated intensity for $T_{e0} < 370$ eV. The fractional abundance of W^{q+} ions presented in Fig. 5 (f) was calculated using ADF11 data (effective ionization coefficients from scd50_w.dat and effective recombination coefficients from acd_w.dat) of OPEN-ADAS [25]. It was assumed that the effective ionization rate of W^{q+} ion, $S(q)$, and the effective recombination rate of W^{q+1} ion, $A(q+1)$, were balanced. In addition, the total tungsten ion density was normalized to 1. By comparing Figs. 5 (b)-(e) and Fig. 5 (f), it is suggested that the UTA spectrum near 200 Å is composed of around W^{20+} ions.

3. Charge State Identification Using CoBIT

In high-temperature plasmas like those found in LHD discharges, a Maxwellian electron distribution behavior is typically observed. This results in an emission spectrum containing peaks from various charge states of both intrinsic and extrinsic impurities, making it challenging to identify and separate these states. In contrast, devices operating on an electron beam with mono energy, such as EBIT, can precisely measure the spectrum of individual charge states of the considered impurity. In an EBIT device, ions are trapped by a magnetic field generated by superconducting magnets and a well-defined electrostatic potential.

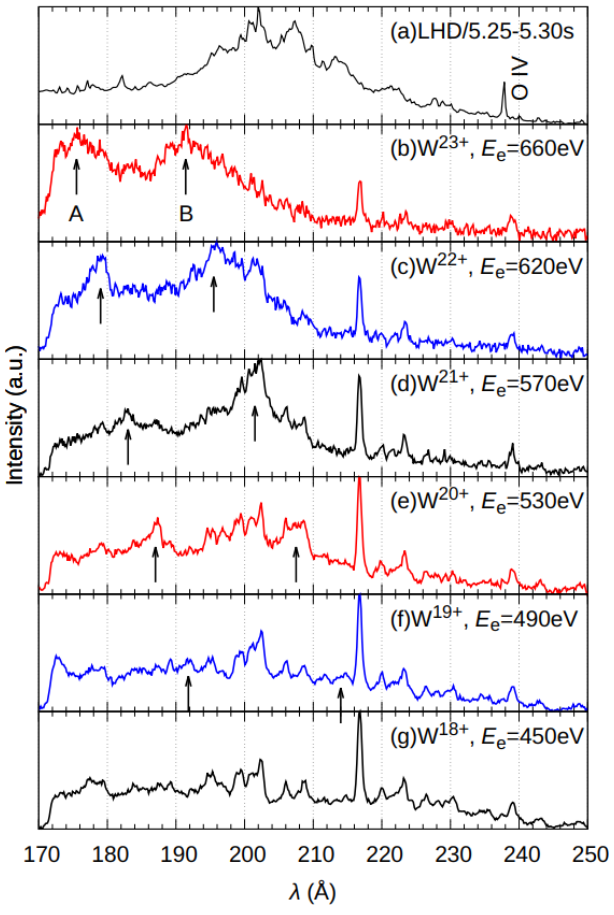

Fig. 6 EUV spectra observed in (a) LHD and (b)-(g) CoBIT of W^{18+}-W^{23+} ions with electron beam energy of 450 - 660 eV.

In this study, we utilized the CoBIT experimental facility at the National Institute for Fusion Science to measure the emission spectra from W^{18+} to W^{23+} ions resulting from the ionization of $W(CO)_6$ gas [16]. CoBIT enables selective measurement of the W^{q+} spectrum by adjusting the electron beam energy, E_e, to an intermediate value between IE(q-1) and IE(q) (i.e. IE(q-1) < E_e < IE(q)), where, IE(q) represents the ionization energy of W^{q+} ion.

Figure 6 shows the tungsten EUV spectra observed in (a) LHD and (b)-(g) CoBIT of W^{18+} - W^{23+} ions with electron beam energy of $450 \leqq E_e \leqq 660$ eV.

The peaks indicated by arrows in each graph in Figs. 6 (b)-(g) correspond to the tungsten ions labeled on the upper right. Two peaks corresponding to the W^{19+}-W^{23+} ions were observed in each spectrum. Here, the observed peaks in the shorter and longer wavelengths are defined as peaks A and B, respectively.

Peaks A and B are considered to correspond to the radiative transition between different excitation states, because the peak wavelength was shifted toward longer wavelengths as the ion charge state decreased. Furthermore, the wavelength of peak B overlapped with that of the EUV spectrum observed in LHD.

4. Identification of Radiative Transition Peaks

We conducted modeling of weighted transition probability, gA, spectra to identify the spectral peaks observed in CoBIT. An integrated software package called Flexile Atomic Code (FAC) was used to calculate the atomic structure and electron-collision parameters, such as energy levels and radiative transition rates, and cross-sections of electron impact excitation, ionization, and recombination [26].

FAC has been widely used for identifying the charge states of numerous atoms/ions and transitions, with observed peaks corresponding to the identified charge states [19, 27, 28].

Energy levels of $4f^m$, $4f^{m-1}$ $5l$ (m = 5 - 10, l = 0 - 4) states of W^{18+}-W^{23+} ions are shown in Fig. 7.

The energies of all excited levels are relative to the ground state ($4f^m$) energy. There are many energy levels for the W^{18+}-W^{23+} ions, most notably the number of energy levels calculated for the W^{20+} ions, which has amounted to about 15,000. The transitions between these levels result in UTA spectrum near 200 Å ($\Delta E \sim 62$ eV).

The gA spectra were synthesized using a Gaussian function with a broadening of 0.2 Å in the full width at half maximum (approximately equal to the instrumental function of the EUV spectrometer used in the LHD experiment).

Figure 8 shows gA spectra of 5s-5p, $5p_{1/2}$-5d, $5p_{3/2}$-5d. 5d-5d, 5f-5g transitions of W^{18+}-W^{23+} ions.

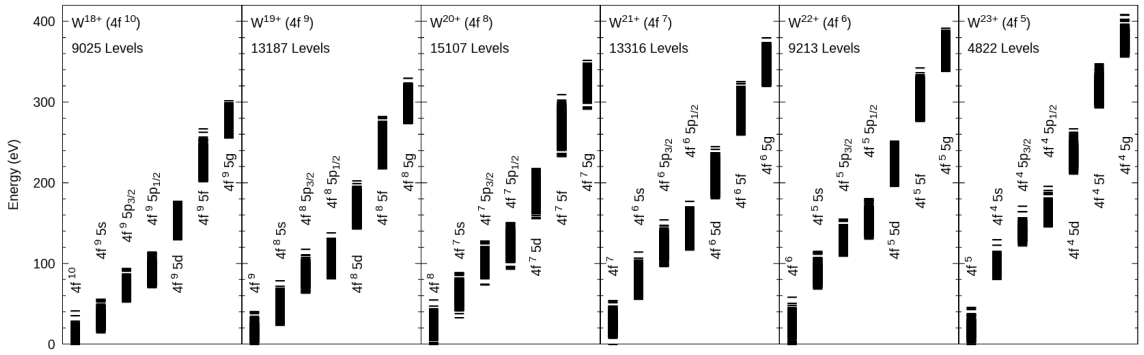

Fig. 7 Energy levels of $4f^m$, $4f^{m-1}$ $5l$ (m = 5 - 10, l = 0 - 4) levels of W^{18+}-W^{23+}.

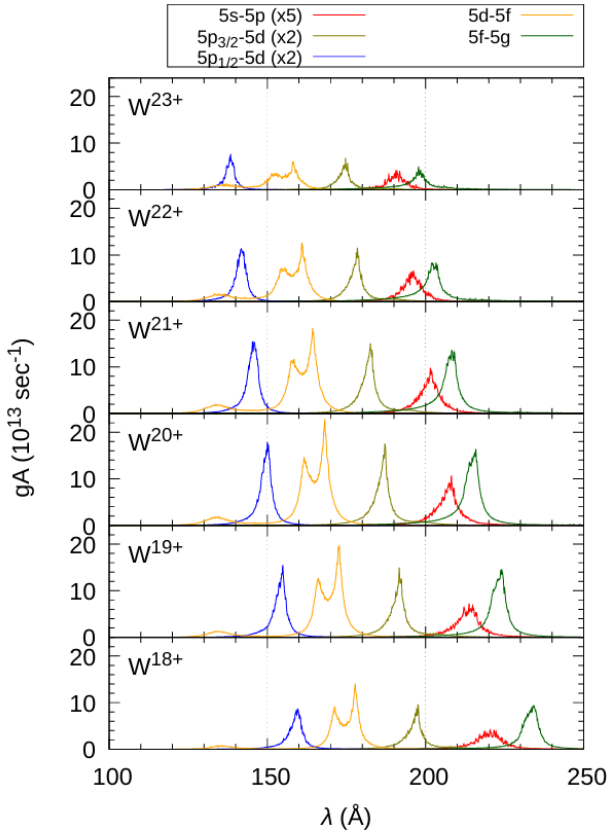

Fig. 8 Weighted transition probability spectra of 5s-5p, $5p_{1/2}$-5d, $5p_{3/2}$-5d, 5d-5f, 5f-5g transition from W^{18+}-W^{23+} ions. These spectra were synthesized using a Gaussian function with a broadening of 0.2 Å in the full width at half maximum.

Primary transitions with principal quantum number n = 5 - 5 (Δn = 0) has a transition probability at a wavelength of 100 - 250 Å. Note that the scales of the gA spectra of 5s-5p and 5p-5d transitions are different from 5d-5f and 5f-5g transitions. The peak wavelength and standard deviation, σ, of the gA spectra were evaluated reference to Refs. [23, 29], using the noncentred nth-order moment, μ_n, defined as

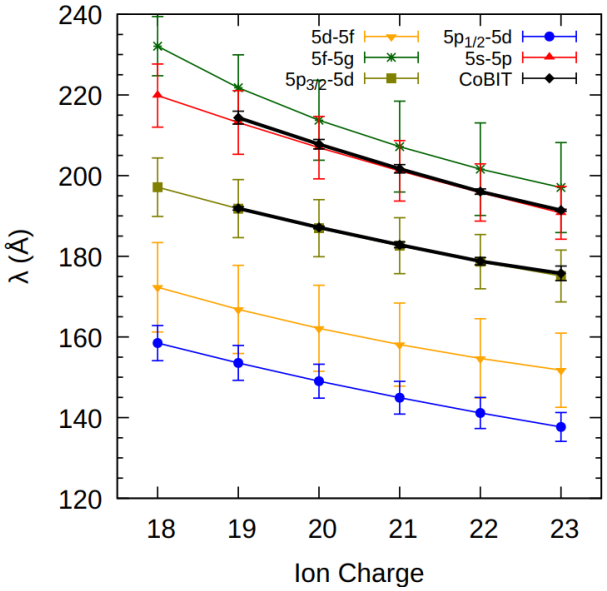

Fig. 9 Wavelength comparison of 5f-5g, 5d-5f, $5p_{3/2}$-5d, $5p_{1/2}$-5d, 5s-5p transitions of W^{19+}-W^{23+} and the peak wavelength observed in CoBIT.

$$\mu_n = \frac{\sum_i \lambda_i^n (gA)_i}{\sum_i (gA)_i}, \quad \sigma = \sqrt{\mu_2 - \mu_1^2}. \tag{1}$$

Where, λ_i and μ_1 represent the transition wavelength and mean peak wavelength, respectively.

Finally, a comparison of the peak wavelengths of CoBIT and the calculated gA spectra is shown in Fig. 9. The wavelength of the peak A and B in Figs. 6 (b)-(f) was determined by applying Gaussian fitting.

It was confirmed that the peak wavelengths from 5s-5p transition of W^{18+}-W^{23+} ions were matched with that of Ref. [23].

Comparing the calculated peak wavelengths of each transition, the peak wavelength observed with CoBIT matched the peak wavelengths of the 5s-5p and $5p_{3/2}$-5d transitions. Therefore, peaks A and B observed in CoBIT correspond to 5s-5p and $5p_{3/2}$-5d transitions, respectively. Furthermore, 5s-5p transitions from W^{19+}-W^{23+} ions ob-

served with CoBIT overlapped with the peaks observed in LHD. Therefore, it is considered that the peaks observed in LHD are mainly composed of 5s-5p transition.

We have successfully separated the charge states included in a tungsten UTA spectra near 200 Å, which is an indicator of the behavior of tungsten ions around W^{20+}. It is expected to be used for impurity diagnostics in ITER edge plasma. In the future, it is necessary to construct a Collisional-Radiative (CR) model to reproduce the observed tungsten UTA spectrum in high-temperature plasmas, taking into account the population of each energy level, and to further improve the charge states identification.

5. Summary

Tungsten UTA spectra were observed near 200 Å in the tungsten pellet injection experiment in LHD. The UTA spectra have a strong intensity with T_{e0} of approximately 300 - 800 eV and include tungsten ions with lower charged states such as W^{20+}. CoBIT experiments were conducted to measure the spectra by separating ion charge states. Two spectral peaks were observed for W^{19+}-W^{23+} ions within CoBIT measurements. These peaks were identified as 5s-5p and $5p_{3/2}$-5d transitions using FAC calculations. Furthermore, 5s-5p transitions from W^{19+}-W^{23+} ions overlapped with the peaks observed in LHD. These spectral peaks are useful for impurity diagnostics of ITER edge plasma.

On the other hand, some strong emission lines were observed at t ~ 4.95 - 5.00 s and T_{e0} ~ 0.83 keV, in Fig. 4. Since the T_{e0} at t ~ 4.95 - 5.00 s is different from 0.3 keV at t ~ 5.25 - 5.30 s, the charge state distribution is assumed to be different as well. Therefore, the strong emission lines are considered to contain ions in higher charge states, such as W^{24+}-W^{30+}. We measured and calculated only for W^{19+}-W^{23+} ions in this present paper. However, it is also very important to identify higher charge states, such as W^{24+}-W^{30+}, as well as lower charge states, such as W^{8+}-W^{18+}. It is necessary to identify the line emission spectra of these ions in the future.

Acknowledgments

The authors thank all the members of the LHD team for their cooperation with the LHD operation.

This work was partially supported by JSPS KAKENHI (Grant Numbers JP20K03896 and JP21H04460), the NIFS Collaboration Research program (Grant Numbers NIFS23KIPP031, NIFS23KIIP021, and NIFS23KIPF007), and JST, the establishment of university fellowships towards the creation of science technology innovation, Grant Number JPMJFS2102. The data supporting the findings of this study are available in the LHD experiment data repository at https://doi.org/10.57451/lhd.analyzed-data.

[1] R.A. Pitts *et al.*, Nucl. Mater. Energy **20**, 100696 (2019).
[2] J. Clemson *et al.*, AIP Conf. Proc. **1525**, 78 (2013).
[3] P. Beiersdorfer *et al.*, J. Phys. B: At. Mol. Opt. Phys. **43**, 144008 (2010).
[4] K. Asmussen *et al.*, Nucl. Fusion **38**, 967 (1998).
[5] R. Neu *et al.*, J. Phys. B: At. Mol. Opt. Phys. **30**, 5057 (1997).
[6] T. Pütterich *et al.*, Plasma Phys. Control. Fusion **50**, 085016 (2008).
[7] J. Yanagibayashi *et al.*, J. Phys. B: At. Mol. Opt. Phys. **43**, 144013 (2010).
[8] T. Nakano *et al.*, Nucl. Fusion **49**, 115204 (2009).
[9] T. Nakano and The JT-60 Team, J. Nucl. Mater. **415**, S327 (2011).
[10] G.J. van Rooij *et al.*, J. Nucl. Mater. **438**, S42 (2013).
[11] L. Zhang *et al.*, Nucl. Inst. Methods Phys. Res. A **916**, 169 (2019).
[12] T. Oishi *et al.*, Atoms **9**, 69 (2021).
[13] M.B. Chowdhuri *et al.*, Plasma Fusion Res. **2**, S1060 (2007).
[14] T. Oishi *et al.*, Phys. Scr. **91**, 025602 (2016).
[15] T. Oishi *et al.*, Phys. Scr. **96**, 025602 (2021).
[16] H.A. Sakaue *et al.*, Phys. Rev. A **92**, 012504 (2015).
[17] Priti *et al.*, Atoms **11**, 57 (2023).
[18] S. Liang *et al.*, Rev. Sci. Instrum. **90**, 093301 (2019).
[19] C.L. Yan *et al.*, Phys. Rev. A **105**, 032820 (2022).
[20] J. Bauche *et al.*, Phys. Scr. **37**, 659 (1988).
[21] A. Kramida *et al.*, http://physics.nist.gov/asd for NIST Atomic Spectra Database (ver. 5.10).
[22] Y. Ralchenko, Plasma Fusion Res. **8**, 2503024 (2013).
[23] C. Suzuki *et al.*, J. Phys. B: At. Mol. Opt. Phys. **44**, 175004 (2011).
[24] M.B. Chowdhuri *et al.*, Rev. Sci. Instrum. **78**, 023501 (2007).
[25] H.P. Summers, The ADAS User Manual, version 2.6 http://www.adas.ac.uk (2004).
[26] M.F. Gu, Astrophys. J. **582**, 1241 (2003).
[27] W. Li *et al.*, Phys. Rev. A **91**, 062501 (2015).
[28] T. Pütterich *et al.*, AIP Conf. Proc. **1545**, 132 (2013).
[29] J. White *et al.*, J. Appl. Phys. **98**, 113301 (2005).